Thermal expansion in dispersion-bound molecular crystals

Hsin-Yu Ko, Robert A. DiStasio, Jr., Biswajit Santra, and Roberto Car

Phys. Rev. Materials **2**, 055603 — Published 18 May 2018

DOI: 10.1103/PhysRevMaterials.2.055603

Thermal Expansion in Dispersion-Bound Molecular Crystals

Hsin-Yu Ko,[1] Robert A. DiStasio Jr.,[2] Biswajit Santra,[1] and Roberto Car[1,3,*]

[1] *Department of Chemistry, Princeton University, Princeton, NJ 08544, USA*
[2] *Department of Chemistry and Chemical Biology, Cornell University, NY 14853, USA*
[3] *Department of Physics, Princeton University, Princeton, NJ 08544, USA*

(Dated: May 2, 2018)

We explore how anharmonicity, nuclear quantum effects (NQE), many-body dispersion interactions, and Pauli repulsion influence thermal properties of dispersion-bound molecular crystals. Accounting for anharmonicity with *ab initio* molecular dynamics yields cell parameters accurate to within 2% of experiment for a set of pyridine-like molecular crystals at finite temperatures and pressures. From the experimental thermal expansion curve, we find that pyridine-I has a Debye temperature just above its melting point, indicating sizable NQE across the entire crystalline range of stability. We find that NQE lead to a substantial volume increase in pyridine-I ($\approx$ 40% more than classical thermal expansion at 153 K) and attribute this to *intermolecular* Pauli repulsion promoted by *intramolecular* quantum fluctuations. When predicting delicate properties such as the thermal expansivity, we show that many-body dispersion interactions and more sophisticated density functional approximations improve the accuracy of the theoretical model.

I. INTRODUCTION

Molecular crystals are versatile materials with widespread use across many fields[1,2], including pharmaceuticals[3], explosives[4], and nonlinear optics[5]. In these cases, properties such as biological activity of a drug, energy density of an explosive, and optical response of a nonlinear medium are all governed by the underlying structures of the molecular crystals and their (often numerous) polymorphs. This stresses the need for accurate and reliable theoretical methods for crystal structure prediction (CSP)[2,6], which not only provide key physical insight into such structure-property relationships, but also offer the promise of rational design of molecular crystals with novel and targeted properties[7].

Despite the fact that all real-world solid-state applications occur at finite temperatures (T) and pressures (p), most CSP methods focus on determining structural properties (*e.g.*, lattice parameters and cell volumes) at 0 K. While such athermal predictions can be accurate for covalent and ionic solids, this approach is unlikely to provide quantitative structural information for non-covalently bound systems such as molecular crystals, which often have large thermal expansivities originating from relatively weak and highly anharmonic intermolecular forces. For example, the volume of the benzene molecular crystal increases by 2.7% from 4 K–138 K[8,9], while thermal effects in Si are at least one order of magnitude smaller at similar temperatures[10].

To predict how finite T and p influence structural properties in molecular crystals, one can utilize *ab initio* molecular dynamics (AIMD)[11] in the isobaric-isothermal (NpT) ensemble. In this technique, the quality of the predicted structures/properties is governed by the accuracy of the theoretical descriptions for the electrons and nuclei. With a quite favorable ratio of cost to accuracy, Density Functional Theory (DFT)[12,13] based on the generalized-gradient approximation (GGA) is often used to treat the electrons and has become the *de facto* standard in first-principles simulations of condensed-phase systems in chemistry, physics, and materials science. Despite this widespread success, semi-local functionals cannot account for long-range dispersion or van der Waals (vdW) interactions, which are crucial for even qualitatively describing non-covalently bound molecular crystals[14]. GGA-based functionals also suffer from spurious self-interaction error (SIE)[15,16], which leads to excessive delocalization of the molecular orbitals and charge densities. To account for non-bonded interactions, various corrections have been incorporated into DFT[17–20], ranging from effective pairwise models[21–24] and approaches that account for many-body dispersion interactions[25–29] to non-local functionals[30–32]. To ameliorate the SIE, hybrid functionals[33] incorporate a fraction of exact exchange in the DFT potential. Beyond the choice of functional, most AIMD simulations employ classical mechanics for the nuclear motion and neglect the quantum mechanical nature of the nuclei as they sample the potential energy surface (PES). Such nuclear quantum effects (NQE), *e.g.*, zero-point motion, can be accounted for using the Feynman path-integral (PI) approach[34–39].

In this work, we explore how anharmonicity, nuclear quantum fluctuations, many-body dispersion interactions, and Pauli repulsion influence structural and thermal properties in dispersion-bound molecular crystals at different thermodynamic conditions. As a first step, we investigate the influence of anharmonicity on the structural properties in a set of pyridine-like molecular crystals (PLMCs), comprised of the following N-heterocyclic aromatic compounds: pyridine (two polymorphs)[40,41], pyrrole[42], pyridazine (two different thermodynamic conditions)[43], and bipyridine[44] (Fig. 1). These molecules are pervasive throughout chemistry, biology, and agriculture[45] as common ligands and solvents, pharmacophores,

* rcar@princeton.edu

and herbicide precursors. To quantify this influence on the PLMC cell parameters under experimental conditions ($T_{\rm expt}$, $p_{\rm expt}$), we performed variable-cell (VC) optimizations at (0 K, $p_{\rm expt}$) and NpT-based AIMD simulations at ($T_{\rm expt}$, $p_{\rm expt}$).

II. COMPUTATIONAL METHODS

For this study, we employed the Perdew-Burke-Ernzerhof (PBE) GGA-based exchange-correlation (XC) functional[46] in conjunction with a fully self-consistent (SC) implementation[24,47] of the Tkatchenko-Scheffler (TS) dispersion correction[22], denoted by PBE+vdW$^{\rm TS}_{\rm SC}$ throughout. The vdW$^{\rm TS}$ method is an effective pairwise (C_6/R^6) approach wherein all atomic parameters (*e.g.*, dipole polarizabilities, vdW radii, and dispersion coefficients) are functionals of the electron density. This approach accounts for the unique chemical environment surrounding each atom and yields interatomic C_6 coefficients accurate to $\approx 5\%$[19,22]. When compared with low-T experiments, VC optimizations with PBE+vdW$^{\rm TS}$ predict lattice parameters to $\approx 2\%$ in crystals containing small organic molecules like ammonia, benzene, urea, and naphthalene[48–50]. In the SC implementation, nonlocal correlation effects are accounted for in the charge density *via* the dispersion contribution to the XC potential. Evaluation of the PBE+vdW$^{\rm TS}_{\rm SC}$ energy and forces ensures appropriate energy conservation during AIMD[47] and can significantly affect binding energies in highly polarizable molecules and materials as well as coinage-metal work functions[24]. The Car-Parrinello molecular dynamics (CPMD)[51] approach was used for all NpT simulations in conjunction with massive Nosé-Hoover thermostat chains[52] and the Parrinello-Rahman barostat[53]. All VC optimizations and CPMD simulations (for ≥ 10 ps) were performed using QUANTUM ESPRESSO (QE)[54,55] at a constant (planewave) kinetic energy cutoff following Bernasconi *et al.*[56] to avoid Pulay-like stress from cell fluctuations. Additional computational details can be found in the Supplemental Material[57].

III. RESULTS AND DISCUSSION

Fig. 1 compares the predicted volumes from VC optimizations and AIMD simulations with experiment, clearly demonstrating that anharmonicity effects are indeed non-negligible in determining this structural property. VC optimizations always underestimate this quantity and the inclusion of anharmonicity *via* NpT-based AIMD systematically reduces the mean absolute error (MAE) from 4.7% to 1.2% in the predicted volumes. In fact, the influence of anharmonicity can be quite substantial in the PLMC set, as evidenced by the 6.4% change in $V_{\rm err}$ for pyridazine at (295 K, 2.7 kBar). We note that the extent to which anharmonicity will influence cell volume expansion depends on a complex interplay between $p_{\rm expt}$

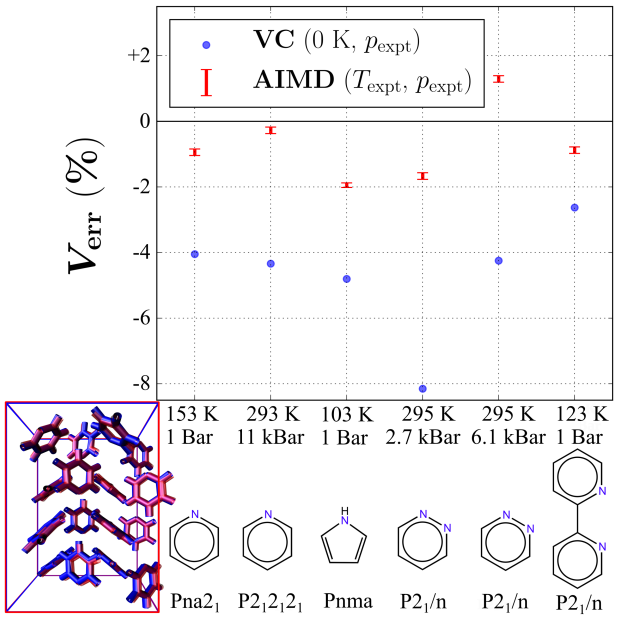

FIG. 1. Predicted cell volumes ($V_{\rm pred}$) from VC optimizations and AIMD simulations using PBE+vdW$^{\rm TS}_{\rm SC}$ for the PLMC set. Errors are defined with respect to experiment ($V_{\rm expt}$) at the indicated thermodynamic conditions as $V_{\rm err} = (V_{\rm pred} - V_{\rm expt})/V_{\rm expt}$. *Inset*: Overlay of predicted (blue) and experimental (red)[40] pyridine-I structures.

and the cohesive forces at work in the crystal (which act together to suppress expansion) and $T_{\rm expt}$ (which provides thermal energy for PES exploration).

AIMD simulations also yield PLMC lattice parameters that agree remarkably well with experiment (Table I). By accounting for anharmonicity, AIMD systematically reduce the MAE in the predicted lattice parameters from 2.0% to 1.3% with respect to experiment. As seen above, VC optimizations tend to underestimate PLMC lattice parameters; however, this trend does not always hold as evidenced by the slight *negative* linear thermal expansion observed along the c axis in pyridine-II. This predicted effect is consistent with the experimental data[41] and reproduces the reference lattice parameter with extremely high fidelity. By considering the lattice parameter fluctuations throughout the AIMD trajectory, we found that the c axis was not the softest (most flexible) dimension in pyridine-II, hence the apparent negative linear thermal expansion in this molecular crystal has a distinctly different origin than that of methanol monohydrate[58]. Since this effect is also observed during GGA-based AIMD (which do not account for dispersion interactions), this phenomenon is most likely electrostatic in nature for pyridine-II. In addition, the structure and orientation of the individual molecules inside the PLMC unit cells are also well described by AIMD with PBE+vdW$^{\rm TS}_{\rm SC}$ (Fig. 1 and Fig. S1), with associated root-mean-square deviations (RMSD) of 0.17 Å across this set

TABLE I. Predicted and experimental structural properties for the PLMC set. All simulations were performed using PBE+vdW$^{\rm TS}_{\rm SC}$ and the numbers in parentheses denote uncertainties in the predicted values. Orthorhombic symmetry was enforced throughout the VC optimizations and AIMD simulations on pyridine-I, pyridine-II, and pyrrole. For all other molecular crystals (as well as the PI-AIMD simulation of pyridine-I) the full cell tensors were allowed to fluctuate. The number of molecules per unit cell and the chosen simulation supercell sizes are also listed along with the RMSD of the atomic positions with respect to experiment.

System	Method	Supercell	a (Å)	b (Å)	c (Å)	α (°)	β (°)	γ (°)	V (Å^3)	$V_{\rm err}$ (%)	RMSD (Å)
Pyridine-I (16 molec)	VC (0 K, 1 Bar)	$1\times1\times1$	17.25	8.88	11.14	90	90	90	1712	−4.0	0.20
	AIMD (153 K, 1 Bar)	$1\times1\times1$	17.43(3)	8.92(2)	11.31(5)	90	90	90	1767(2)	−0.9(1)	0.14
	PI-AIMD (153 K, 1 Bar)	$1\times1\times1$	17.51(4)	8.95(3)	11.44(6)	90.0(1)	89.5(3)	90.02(7)	1789(2)	+0.3(1)	0.13
	Expt.[40]	–	17.52	8.97	11.35	90	90	90	1784	–	–
Pyridine-II (4 molec)	VC (0 K, 11 kBar)	$2\times2\times1$	5.33	6.56	11.30	90	90	90	396.0	−4.3	0.19
	AIMD (298 K, 11 kBar)	$2\times2\times1$	5.46(1)	6.72(4)	11.23(5)	90	90	90	412.8(5)	−0.4(1)	0.10
	Expt.[41]	–	5.40	6.80	11.23	90	90	90	414.0	–	–
Pyrrole (4 molec)	VC (0 K, 1 Bar)	$2\times1\times3$	7.23	10.10	4.96	90	90	90	361.9	−4.8	0.21
	AIMD (103 K, 1 Bar)	$2\times1\times3$	7.35(2)	10.19(1)	4.99(1)	90	90	90	372.8(3)	−1.99(7)	0.18
	Expt.[42]	–	7.29	10.29	5.07	90	90	90	380.2	–	–
Pyridazine (4 molec)	VC (0 K, 2.7 kBar)	$3\times1\times1$	3.675	10.62	9.70	90.1	91.4	90.0	378.4	−8.2	0.26
	AIMD (295 K, 2.7 kBar)	$3\times1\times1$	3.809(5)	10.86(2)	9.83(1)	90.0(1)	90.6(3)	90.1(2)	405.1(5)	−1.7(1)	0.21
	Expt.[43]	–	3.843	10.96	9.78	90.0	91.1	90.0	412.0	–	–
Pyridazine (4 molec)	VC (0 K, 6.1 kBar)	$3\times1\times1$	3.643	10.53	9.68	90.2	90.8	90.0	370.4	−4.3	0.20
	AIMD (295 K, 6.1 kBar)	$3\times1\times1$	3.735(6)	10.76(3)	9.79(2)	89.9(2)	90.5(4)	89.9(2)	391.9(5)	1.3(1)	0.24
	Expt.[43]	–	3.719	10.75	9.68	90.0	91.5	90.0	386.9	–	–
Bipyridine (2 molec)	VC (0 K, 1 Bar)	$2\times2\times1$	5.529	5.98	11.58	90.00	96.46	90.00	380.7	−2.6	0.18
	AIMD (123 K, 1 Bar)	$2\times2\times1$	5.576(6)	5.99(1)	11.67(2)	90.01(5)	95.91(9)	90.07(9)	387.6(4)	−0.9(1)	0.15
	Expt.[44]	–	5.486	6.17	11.61	90.00	95.28	90.00	391.0	–	–

of dispersion-bound molecular crystals.

Based on these findings, we conclude that structural predictions are significantly improved when anharmonicity is accounted for *via* NpT-based AIMD simulations, yielding *finite-temperature* structural properties in dispersion-bound molecular crystals that are within 2% of experiment. However, the results reported herein still systematically underestimate the experimental PLMC cell volumes. For more accurate and reliable predictions, we find that NQE (such as zero-point fluctuations), many-body dispersion interactions, and Pauli repulsion all have a non-negligible influence over the structural and thermal properties of dispersion-bound molecular crystals. To demonstrate this, we now focus our attention on a detailed case study of the pyridine-I polymorph.

While AIMD simulations are able to furnish accurate structural properties for the PLMCs across a range of thermodynamic conditions, the shape of the thermal expansion curve for deuterated pyridine-I from neutron powder diffraction experiments[41] significantly differs from our theoretical predictions (Fig. 2). In this regard, the predicted $V(T)$ curve is linear across the entire T range considered (*i.e.*, 12 K–153 K at $p_{\rm expt} = 1$ Bar), reflecting the use of classical mechanics for the nuclear motion. The experimental curve, on the other hand, shows non-linear behavior in this T interval, with significant deviations from linearity at low temperatures, *i.e.*, for $T \leq 50$ K. This observation strongly indicates that NQE (in particular zero-point motion) play a non-negligible role in governing the structural and thermal properties of this dispersion-bound molecular crystal.

To gain further insight into the thermal expansion behavior in this system, we utilize the Debye model, which is an isotropic acoustic approximation for the phonons in a solid. Within this framework, $V(T)$ can be derived from the corresponding Gibbs free energy (at a given p) as[57]:

$$V(T) = V(0) + \left[3Nk_B\frac{\Theta'_D}{\Theta_D}\,\mathbf{D}\!\left(\frac{\Theta_D}{T}\right)\right]T, \qquad (1)$$

in which $V(0)$ is the cell volume at 0 K, N is the number of atoms, $\Theta_D = \Theta_D(p)$ is the Debye temperature, $\Theta'_D = \mathrm{d}\,\Theta_D(p)/\mathrm{d}\,p$ is the pressure derivative of Θ_D (which accounts for anharmonicity in the underlying PES), and $\mathbf{D}(\cdot)$ is the Debye function[59]. Quite interestingly, we find that the experimental thermal expansion curve for C_5D_5N can be fit rather well with Eq. (1), as shown by the purple line in Fig. 2 (and Fig. S2). A similarly good fit using the Debye interpolation formula was obtained for the methanol monohydrate molecular crystal[58]. The validity of the Debye model for thermal expansion in pyridine-I is further supported by the physical value for the Debye temperature obtained from the fit, namely, $\Theta_D = 235(5)$ K. This corresponds to an average sound velocity of 1710 m/s in this system, which falls within the experimentally determined range for the sound velocity of the closely related benzene molecular crystal[57,60].

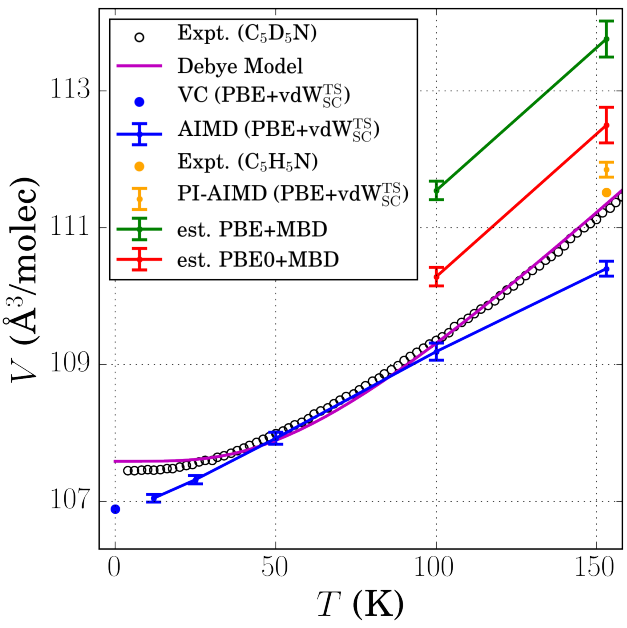

FIG. 2. Predicted and experimental thermal expansion curves for pyridine-I. Experimental data is included for pyridine-I (C_5H_5N, gold circle), from single-crystal X-ray diffraction[40], and fully deuterated pyridine-I (C_5D_5N, open black circles), from neutron powder diffraction[41]. A fit of the experimental thermal expansion curve for deuterated pyridine-I using the Debye model for $V(T)$ is given by the purple line (Eq. (1)). Theoretical data is included for VC optimizations (blue circle), AIMD simulations (blue line), and PI-AIMD simulations (gold circle with error bar) at the PBE+vdW$^{TS}_{SC}$ level; estimated PBE+MBD results (green line, Eq. (4)); estimated PBE0+MBD results (red line, see text for details).

The fact that Θ_D is slightly above the melting temperature of pyridine-I ($T_m = 232$ K) suggests that NQE should have a sizable influence across the entire crystalline range of stability in this polymorph. To directly confirm the importance of NQE in determining the structure of pyridine-I, we performed a PI-AIMD simulation using PBE+vdW$^{TS}_{SC}$ at (153 K, 1 Bar)[38,39,57,61]. When compared to the 3% volume expansion due to classical thermal fluctuations (*cf.* the difference between the VC optimization at 0 K and AIMD simulation at 153 K, see Table I), we find that the inclusion of NQE results in an additional 1.2% expansion in the cell volume. This change is quite sizable ($\approx 40\%$ of the classical thermal expansion) and further reduces $V_{\rm err}$ in pyridine-I to +0.3% with respect to experiment.

To investigate how NQE lead to such an appreciable change in the pyridine-I cell volume, we first analyze how nuclear quantum fluctuations affect rigid molecular motions, *i.e.*, translations and librations, in this molecular crystal. To quantify these effects, we compute the corresponding temperature correction (ΔT) from the leading-order quantum correction to the momentum distribution for a Cartesian coordinate (q) corresponding to the molecular center of mass[59,62]:

$$\Delta T = \frac{\hbar^2}{12MT^2}\,\langle F_q^2\rangle\,, \qquad (2)$$

in which M is the molecular mass and $\langle F_q^2\rangle$ is the mean-square force along q obtained by statistically averaging over the classical AIMD trajectory[63]. In doing so, we find that $\Delta T \approx 10$ K for the rigid translational and librational modes in this system. However, the additional thermal expansion due to NQE corresponds to a temperature elevation of ≈ 50 K (assuming linear thermal expansion for $T \geq 153$ K), which is higher than the contributions from such rigid molecular motions and indicative of an additional mechanism for the observed expansion in pyridine-I.

To further understand the origin of this NQE-induced volume expansion, we computed a series of *intermolecular* pair-correlation functions involving the peripheral atoms on each pyridine molecule ($g_{\rm HH}(r)$, $g_{\rm CH}(r)$, $g_{\rm NH}(r)$) based on AIMD and PI-AIMD simulations of this non-covalently bound molecular crystal (Fig. 3). From these plots, one can immediately see that the inclusion of NQE—which cause individual pyridine molecules to fluctuate to a larger extent—lead to shorter intermolecular contacts (and hence more charge density overlap) among neighboring molecules in pyridine-I. For instance, the peripheral H atoms on neighboring pyridine molecules are closer by ≈ 0.2 Å, and the probability of finding these two H atoms at a distance shorter than the sum of their vdW radii[64] ($r = 2.4$ Å) is enhanced by 28% when accounting for NQE. With atom pairs located within their respective vdW envelope, there will be an increase in the Pauli repulsion experienced by neighboring pyridine molecules, which in turn leads to a larger equilibrium cell volume in the molecular crystal[65]. These findings hold for all atom pairs considered and demonstrate that *intermolecular* Pauli repulsion promoted by *intramolecular* quantum fluctuations is the dominant physical mechanism responsible for the observed cell volume increases in pyridine-I due to NQE.

Considering now the thermal expansivity (or thermal expansion coefficient),

$$\alpha(T) = \frac{1}{V(T)}\left(\frac{\partial V(T)}{\partial T}\right)_p\,, \qquad (3)$$

we determined an experimental value of $\alpha = 3.5 \times 10^{-4}$ K^{-1} for pyridine-I at (153 K, 1 Bar) based on the C_5D_5N thermal expansion curve[41]. This value agrees quite well with the analytical finding from the Debye interpolation, *i.e.*, $\alpha = 3.7 \times 10^{-4}$ K^{-1}, further illustrating the utility of this model in describing this system. However, the α value from classical AIMD simulations using PBE+vdW$^{TS}_{SC}$ ($\alpha = 2.1 \times 10^{-4}$ K^{-1}) significantly underestimates the experimental value by $\approx 40\%$. Since cohesion in pyridine-I is dominated by dispersion interactions (Table S1 and Fig. S3), this suggests that PBE+vdW$^{TS}_{SC}$ overestimates the cohesive forces at work in this non-

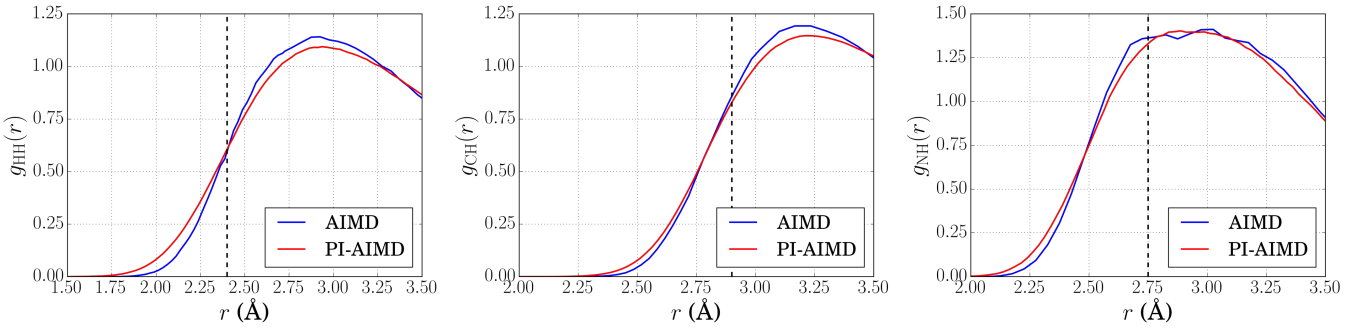

FIG. 3. Comparison of the *intermolecular* HH, CH, and NH pair-correlation functions obtained from AIMD (blue) and PI-AIMD (red) simulations of pyridine-I using PBE+vdW$^{\mathrm{TS}}_{\mathrm{SC}}$. Dashed vertical lines represent the sum of the van der Waals (vdW) radii[64] for the respective pair of atoms.

TABLE II. Thermal expansivity (α) values for pyridine-I at (153 K, 1 Bar) from theoretical simulations (at the PBE+vdW$^{\mathrm{TS}}_{\mathrm{SC}}$, est. PBE+MBD, and est. PBE0+MBD levels), the Debye model, and experiment. Errors are reported with respect to the experimental value and the numbers in parentheses denote uncertainties in α.

Pyridine-I	α (10^{-4} K^{-1})	α_{err} (%)
PBE+vdW$^{\mathrm{TS}}_{\mathrm{SC}}$	2.1(3)	−40.0
est. PBE+MBD	3.7(5)	+5.7
est. PBE0+MBD	3.7(5)	+5.7
Debye Model	3.65(4)	+4.3
Expt.[41]	3.5(1)	–

covalently bound molecular crystal. This finding is consistent with other studies on molecular crystal lattice energies with this method[50]. As such, we now investigate how a more comprehensive treatment of the beyond-pairwise many-body dispersion forces impacts our prediction of this thermal property in pyridine-I.

Beyond-pairwise dispersion interactions include terms such as the three-body Axilrod-Teller-Muto (ATM) contribution (C_9/R^9)[66,67], which is more short-ranged than the C_6/R^6 term in the effective-pairwise vdW$^{\mathrm{TS}}$ level and often provides a repulsive contribution to the binding energy. Since the inclusion of the ATM term alone is usually not sufficient to describe the full many-body expansion of the dispersion energy[68], we employ the many body dispersion (MBD) model[25–29] to investigate how these higher-order non-bonded interactions affect the structural and thermal properties in pyridine-I. The MBD approach furnishes a description of all N-body dispersion energy contributions by mapping the atoms comprising the system onto a set of coupled quantum harmonic oscillators, and then computing the long-range correlation energy in the random-phase approximation (RPA)[27,28,69]. When coupled with DFT, MBD has been shown to provide an accurate and reliable description of the non-covalent interactions in molecules and materials[19], ranging from molecular crystals[50,70,71] to complex polarizable nanostructures[72,73].

To account for many-body dispersion interactions, we estimated[74] the average cell volume at the PBE+MBD level ($\langle V\rangle_{\mathrm{MBD}}$) by Boltzmann reweighting the configurations from the PBE+vdW$^{\mathrm{TS}}_{\mathrm{SC}}$ trajectory, *i.e.*,

$$\langle V\rangle_{\mathrm{MBD}} = \frac{\langle V \exp\left[-\beta\left(U_{\mathrm{MBD}} - U_{\mathrm{TS}}\right)\right]\rangle_{\mathrm{TS}}}{\langle \exp\left[-\beta\left(U_{\mathrm{MBD}} - U_{\mathrm{TS}}\right)\right]\rangle_{\mathrm{TS}}}, \qquad (4)$$

in which β is the inverse temperature, U_{TS} and U_{MBD} are the corresponding dispersion energies from these two methods, and $\langle\cdot\rangle_{\mathrm{TS}}$ represents a statistical average over the PBE+vdW$^{\mathrm{TS}}_{\mathrm{SC}}$ ensemble[57]. The resulting estimates for $\langle V\rangle_{\mathrm{MBD}}$ are shown in Fig. 2 and were used to determine that $\alpha = 3.7\times10^{-4}$ K^{-1} at the PBE+MBD level, which is in significantly better agreement with the experimental value than PBE+vdW$^{\mathrm{TS}}_{\mathrm{SC}}$ (Table II). However, the estimated PBE+MBD cell volumes are noticeably larger than experiment, with predictions that are now less accurate than PBE+vdW$^{\mathrm{TS}}_{\mathrm{SC}}$. This may be due, in part, to the perturbative estimate of the PBE+MBD cell volumes using Eq. (4). Since MBD provides a more comprehensive treatment of dispersion interactions[17,19], this can also be indicative of other deficiencies present in the XC functional.

Hybrid functionals such as PBE0[75], which include a fraction of exact exchange, have been found to be more accurate overall than PBE in the treatment of molecular crystals[50]. In the pyridine-I molecular crystal, we find that PBE0+vdW$^{\mathrm{TS}}_{\mathrm{SC}}$[47,76,77] predicts a reduction in the 0 K cell volume by $\Delta V = -1.02$ Å^3/molec when compared to PBE+vdW$^{\mathrm{TS}}_{\mathrm{SC}}$. This effect likely originates from a combination of small changes in the molecular geometries as well as a better treatment of Pauli repulsion between neighboring molecules. Hence, we estimate the PBE0+MBD volume by adding this constant shift to the PBE+MBD results above (Fig. 2). This largely corrects the overestimation of the cell volume with PBE+MBD, and the resulting estimated PBE0+MBD values are now in better agreement with both the experimental volume

(on an absolute scale) and the thermal expansivity. We stress here that an improved theoretical description of the Pauli repulsion might be of particular importance when simultaneously accounting for NQE, which increase the amount of charge density overlap among neighboring molecules in pyridine-I.

IV. CONCLUSIONS

In this work, we explored how a complex interplay between anharmonicity, NQE, many-body dispersion interactions, and Pauli repulsion influence the structural and thermal properties of dispersion-bound molecular crystals. By focusing on pyridine-I, we showed that the Debye model is well-suited to describe the thermal expansion behavior in this system across the range of available experimental temperatures. With a Debye temperature just above the melting point, we expect that NQE will be sizable across the entire crystalline range of stability in this polymorph. At low T, PI-AIMD simulations become computationally intractable (due to the steep increase in the required Trotter dimension) and it would be more efficient to include NQE *via* the quasiharmonic or self-consistent harmonic approximations[78–80]. Based on our detailed case study of the pyridine-I molecular crystal, we expect that the qualitative trends outlined herein are robust and transferable to other dispersion-bound molecular crystals. In this regard, a logical extension of this work would include a fully self-consistent treatment of the pyridine-I molecular crystal (as well as other important non-covalently bound molecular crystals) that accounts for NQE as well as an improved description of the underlying electronic structure. Beyond the structural and thermal properties considered herein, the existence of thermodynamically relevant polymorphs further advocates for the determination of structures, stabilities, and properties of molecular crystals under NpT conditions. Based on the findings presented in this work, free energy calculations that simultaneously account for nuclear quantum fluctuations and many-body dispersion interactions within a DFT scheme with reduced SIE will be required for an accurate and reliable description of dispersion-bound molecular crystals.

ACKNOWLEDGMENTS

The authors thank Nandini Ananth and Igor Poltavsky for useful scientific discussions. All authors gratefully acknowledge support from the U.S. Department of Energy under Grant Nos. DE-SC0005180 and DE-SC0008626. R.D. acknowledges partial support from Cornell University through start-up funding and the Cornell Center for Materials Research (CCMR) with funding from the National Science Foundation MRSEC program (DMR-1719875). This research used resources of the National Energy Research Scientific Computing (NERSC) Center, which is supported by the Office of Science of the U.S. Department of Energy under Contract No. DE-AC02-05CH11231. This research used resources of the Argonne Leadership Computing Facility at Argonne National Laboratory, which is supported by the Office of Science of the U.S. Department of Energy under Contract No. DE-AC02-06CH11357. Additional resources were provided by the Terascale Infrastructure for Groundbreaking Research in Science and Engineering (TIGRESS) High Performance Computing Center and Visualization Laboratory at Princeton University.

[1] J. Bernstein, *Polymorphism in Molecular Crystals* (Oxford University Press, New York, 2007).
[2] S. L. Price, Int. Rev. Phys. Chem. **27**, 541 (2008).
[3] Ö. Almarsson and M. J. Zaworotko, Chem. Commun. **0**, 1889 (2004).
[4] L. E. Fried, M. R. Manaa, P. F. Pagoria, and R. L. Simpson, Annu. Rev. Mater. Sci. **31**, 291 (2001).
[5] M. J. Prakash and T. P. Radhakrishnan, Chem. Mater. **18**, 2943 (2006).
[6] S. L. Price, Phys. Chem. Chem. Phys. **10**, 1996 (2008).
[7] J. Hoja, A. M. Reilly, and A. Tkatchenko, WIREs Comput Mol Sci **7**, 1294 (2017).
[8] W. I. F. David, R. M. Ibberson, G. A. Jeffrey, and J. R. Ruble, Physica B (Amsterdam, Neth.) **180-181**, 597 (1992).
[9] G. E. Bacon, N. A. Curry, and S. A. Wilson, Proc. R. Soc. Lond. A **279**, 98 (1964).
[10] T. Middelmann, A. Walkov, G. Bartl, and R. Schödel, Phys. Rev. B **92**, 174113 (2015).
[11] D. Marx and J. Hutter, *Ab Initio Molecular Dynamics: Basic Theory and Advanced Methods* (Cambridge University Press, Cambridge, 2009).
[12] P. Hohenberg and W. Kohn, Phys. Rev. **136**, B864 (1964).
[13] W. Kohn and L. J. Sham, Phys. Rev. **140**, A1133 (1965).
[14] D. Lu, Y. Li, D. Rocca, and G. Galli, Phys. Rev. Lett. **102**, 206411 (2009).
[15] J. P. Perdew and A. Zunger, Phys. Rev. B **23**, 5048 (1981).
[16] A. J. Cohen, P. Mori-Sánchez, and W. Yang, Science **321**, 792 (2008).
[17] J. Klimeš and A. Michaelides, J. Chem. Phys. **137**, 120901 (2012).
[18] S. Grimme, A. Hansen, J. G. Brandenburg, and C. Bannwarth, Chem. Rev. **116**, 5105 (2016).
[19] J. Hermann, R. A. DiStasio Jr., and A. Tkatchenko, Chem. Rev. **117**, 4714 (2017).
[20] K. Berland, V. R. Cooper, K. Lee, E. Schröder, T. Thonhauser, P. Hyldgaard, and B. I. Lundqvist, Rep. Prog. Phys. **78**, 066501 (2015).
[21] A. D. Becke and E. R. Johnson, J. Chem. Phys. **127**, 154108 (2007).
[22] A. Tkatchenko and M. Scheffler, Phys. Rev. Lett. **102**, 073005 (2009).

[23] S. Grimme, J. Antony, S. Ehrlich, and H. Krieg, J. Chem. Phys. **132**, 154104 (2010).
[24] N. Ferri, R. A. DiStasio Jr., A. Ambrosetti, R. Car, and A. Tkatchenko, Phys. Rev. Lett. **114**, 176802 (2015).
[25] A. Tkatchenko, R. A. DiStasio Jr., R. Car, and M. Scheffler, Phys. Rev. Lett. **108**, 236402 (2012).
[26] R. A. DiStasio Jr., O. A. von Lilienfeld, and A. Tkatchenko, Proc. Natl. Acad. Sci. USA **109**, 14791 (2012).
[27] R. A. DiStasio Jr., V. V. Gobre, and A. Tkatchenko, J. Phys.: Condens. Matter **26**, 213202 (2014).
[28] A. Ambrosetti, A. M. Reilly, R. A. DiStasio Jr., and A. Tkatchenko, J. Chem. Phys. **140**, 18A508 (2014).
[29] M. A. Blood-Forsythe, T. Markovich, R. A. DiStasio Jr., R. Car, and A. Aspuru-Guzik, Chem. Sci. **7**, 1712 (2016).
[30] M. Dion, H. Rydberg, E. Schröder, D. C. Langreth, and B. I. Lundqvist, Phys. Rev. Lett. **92**, 246401 (2004).
[31] O. A. Vydrov and T. Van Voorhis, Phys. Rev. Lett. **103**, 063004 (2009).
[32] K. Lee, É. D. Murray, L. Kong, B. I. Lundqvist, and D. C. Langreth, Phys. Rev. B **82**, 081101 (2010).
[33] A. D. Becke, J. Chem. Phys. **98**, 1372 (1993).
[34] L. D. Fosdick, J. Math Phys. **3**, 1251 (1962).
[35] D. Chandler and P. G. Wolynes, J. Chem. Phys. **74**, 4078 (1981).
[36] D. Marx and M. Parrinello, J. Chem. Phys. **104**, 4077 (1996).
[37] M. E. Tuckerman, D. Marx, M. L. Klein, and M. Parrinello, J. Chem. Phys. **104**, 5579 (1996).
[38] M. Ceriotti, D. E. Manolopoulos, and M. Parrinello, J. Chem. Phys. **134**, 084104 (2011).
[39] M. Ceriotti, J. More, and D. E. Manolopoulos, Comput. Phys. Commun. **185**, 1019 (2014).
[40] D. Mootz and H.-G. Wussow, J. Chem. Phys. **75**, 1517 (1981).
[41] S. Crawford, M. T. Kirchner, D. Bläser, R. Boese, W. I. F. David, A. Dawson, A. Gehrke, R. M. Ibberson, W. G. Marshall, S. Parsons, et al., Angew. Chem. Int. Ed. **48**, 755 (2009).
[42] R. Goddard, O. Heinemann, and C. Krüger, Acta Crystallogr., Sect. C: Cryst. Struct. Commun. **53**, 1846 (1997).
[43] M. Podsiadło, K. Jakóbek, and A. Katrusiak, Cryst. Eng. Comm. **12**, 2561 (2010).
[44] F. E. Kühn, M. Groarke, É. Bencze, E. Herdtweck, A. Prazeres, A. M. Santos, M. J. Calhorda, C. C. Romão, I. S. Gonçalves, A. D. Lopes, et al., Chem. Eur. J. **8**, 2370 (2002).
[45] Gilchrist, *Heterocyclic Chemistry* (Pearson Education, Essex, 2007).
[46] J. P. Perdew, K. Burke, and M. Ernzerhof, Phys. Rev. Lett. **77**, 3865 (1996).
[47] R. A. DiStasio Jr., B. Santra, Z. Li, X. Wu, and R. Car, J. Chem. Phys. **141**, 084502 (2014).
[48] W. A. Al-Saidi, V. K. Voora, and K. D. Jordan, J. Chem. Theory Comput. **8**, 1503 (2012).
[49] T. Bučko, S. Lebègue, J. Hafner, and J. G. Ángyán, Phys. Rev. B **87**, 064110 (2013).
[50] A. M. Reilly and A. Tkatchenko, J. Chem. Phys. **139**, 024705 (2013).
[51] R. Car and M. Parrinello, Phys. Rev. Lett. **55**, 2471 (1985).
[52] D. J. Tobias, G. J. Martyna, and M. L. Klein, J. Phys. Chem. **97**, 12959 (1993).
[53] M. Parrinello and A. Rahman, Phys. Rev. Lett. **45**, 1196 (1980).
[54] P. Giannozzi, S. Baroni, N. Bonini, M. Calandra, R. Car, C. Cavazzoni, D. Ceresoli, G. L. Chiarotti, M. Cococcioni, I. Dabo, et al., J. Phys.: Condens. Matter **21**, 395502 (2009).
[55] P. Giannozzi, O. Andreussi, T. Brumme, O. Bunau, M. B. Nardelli, M. Calandra, R. Car, C. Cavazzoni, D Ceresoli, M. Cococcioni, et al., J. Phys.: Condens. Matter **29**, 465901 (2017).
[56] M. Bernasconi, G. Chiarotti, P. Focher, S. Scandolo, E. Tosatti, and M. Parrinello, J. Phys. Chem. Solids **56**, 501 (1995).
[57] See Supplemental Material at [URL will be inserted by publisher] for simulation details, overlays of the predicted and experimental PLMC structures, derivation of $V(T)$ for pyridine-I in the Debye model, estimation of the average sound velocity in pyridine-I, and analysis of the molecular dipoles and cohesive interactions in the PLMC set.
[58] A. D. Fortes, E. Suard, and K. S. Knight, Science **331**, 742 (2011).
[59] L. D. Landau and E. M. Lifshitz, *Statistical Physics* (Elsevier, Singapore, 1996).
[60] J. C. W. Heseltine and D. W. Elliot, Master's thesis, U.S. Naval Postgraduate School, Monterey, California (1962).
[61] M. Ceriotti, G. Bussi, and M. Parrinello, Phys. Rev. Lett. **103**, 030603 (2009).
[62] I. Poltavsky, R. A. DiStasio Jr., and A. Tkatchenko, J. Chem. Phys. **148**, 102325 (2017).
[63] Similar temperature corrections can be derived for librational motions (assuming rigid molecular structures) as $\Delta T = \frac{\hbar^2}{12 I_j T^2} \langle \tau_j^2 \rangle$, in which I_j is the associated moment of inertia and τ_j is the torque along the corresponding principal rotational axis, ϕ_j.
[64] A. Bondi, J. Phys. Chem. **68**, 441 (1964).
[65] A consistent picture is also provided by a Voronoi analysis of the AIMD and PI-AIMD trajectories to quantify the size of the fluctuating pyridine molecules. Here, we find that nuclear quantum fluctuations enlarge the average molecular size from 110.6 Å^3 (AIMD) to 111.7 Å^3 (PI-AIMD), with a corresponding increase in the associated standard deviation from 2.6 Å^3 to 2.9 Å^3.
[66] B. M. Axilrod and E. Teller, J. Chem. Phys. **11**, 299 (1943).
[67] Y. Muto, Proc. Phys. Math. Soc. Jpn. **17**, 629 (1943).
[68] A. Ambrosetti, D. Alfè, R. A. DiStasio Jr., and A. Tkatchenko, J. Phys. Chem. Lett. **5**, 849 (2014).
[69] A. Tkatchenko, A. Ambrosetti, and R. A. DiStasio Jr., J. Chem. Phys. **138**, 074106 (2013).
[70] N. Marom, R. A. DiStasio Jr., V. Atalla, S. Levchenko, A. M. Reilly, J. R. Chelikowsky, L. Leiserowitz, and A. Tkatchenko, Angew. Chem. Int. Ed. **52**, 6629 (2013).
[71] A. M. Reilly, R. I. Cooper, C. S. Adjiman, S. Bhattacharya, A. D. Boese, J. G. Brandenburg, P. J. Bygrave, R. Bylsma, J. E. Campbell, R. Car, et al., Acta Crystallogr., Sect. B: Struct. Sci. **72**, 439 (2016).
[72] A. Ambrosetti, N. Ferri, R. A. DiStasio Jr., and A. Tkatchenko, Science **351**, 1171 (2016).
[73] A. Ambrosetti, P. L. Silvestrelli, and A. Tkatchenko, Phys. Rev. B **95**, 235417 (2017).
[74] At the current time, analytical and on-the-fly evaluation of the ionic and cell forces at the MBD level were not available in the existing implementation of this scheme and these limitations will be addressed in future work.

[75] J. P. Perdew, M. Ernzerhof, and K. Burke, J. Chem. Phys. **105**, 9982 (1996).
[76] X. Wu, A. Selloni, and R. Car, Phys. Rev. B **79**, 085102 (2009).
[77] H.-Y. Ko, J. Jia, B. Santra, X. Wu, R. Car, and R. A. DiStasio Jr., *Enabling large-scale hybrid density functional theory calculations in the condensed phase*, (in preparation).
[78] D. J. Hooton, Phil. Mag. Ser. 7 **46**, 422 (1955).
[79] I. Errea, M. Calandra, and F. Mauri, Phys. Rev. Lett. **111**, 177002 (2013).
[80] I. Errea, M. Calandra, and F. Mauri, Phys. Rev. B **89**, 064302 (2014).